Dynamic structure function of a cold Fermi gas at unitarity

2014 J. Phys.: Conf. Ser. 529 012009

(http://iopscience.iop.org/1742-6596/529/1/012009)

Journal of Physics: Conference Series **529** (2014) 012009 doi:10.1088/1742-6596/529/1/012009

Dynamic structure function of a cold Fermi gas at unitarity

G E Astrakharchik[‡], J Boronat[‡], E Krotscheck[+†] and T Lichtenegger[+†]

[‡]Departament de Física i Enginyeria Nuclear, Campus Nord B4-B5, Universitat Politècnica de Catalunya, E-08034 Barcelona, Spain
[+]Department of Physics, University at Buffalo, SUNY Buffalo NY 14260
[†]Institut für Theoretische Physik, Johannes Kepler Universität, A 4040 Linz, Austria

E-mail: eckhard.krotscheck@jku.at

Abstract. We present a theoretical study of the dynamic structure function of a resonantly interacting two-component Fermi gas at zero temperature. Our approach is based on dynamic many-body theory able to describe excitations in strongly correlated Fermi systems. The fixed-node diffusion Monte Carlo method is used to produce the ground-state correlation functions which are used as an input for the excitation theory. Our approach reproduces recent Bragg scattering data in both the density and the spin channel. In the BCS regime, the response is close to that of the ideal Fermi gas. On the BEC side, the Bose peak associated with the formation of dimers dominates the density channel of the dynamic response. When the fraction of dimers is large our theory departs from the experimental data, mainly in the spin channel.

1. Introduction

An impressive advance in realizing and controlling ultracold Fermi gases has permitted to study physical phenomena whose appearance was previously only a matter of speculation [1]. One of the major advances has been the first clean observation of a crossover between two limits of Fermi matter, the Bose-Einstein condensate (BEC) regime composed by Fermi molecules and the Bardeen-Cooper-Schrieffer (BCS) superfluid gas where Cooper pairs are formed [2, 3, 4, 5].

In the dilute limit, interactions between atoms can be described by a single parameter, namely the s-wave scattering length a. The system evolves from a BCS regime with no bound state ($a < 0$) to a molecular one (BEC) with a two-body bound state ($a > 0$), crossing a singular point where $|a| \to \infty$ corresponding to a Fano-Feshbach resonance [6, 7, 8]. This special point is referred to as the unitary limit and is expected to show a number of universal properties. Indeed, in this regime the only relevant

length and energy scales are the inverse Fermi momentum k_F^{-1} and the Fermi energy $E_{\rm F}$, respectively.

Nowadays, the unitary Fermi gas is routinely realized in experiments. An accurate theoretical description of the unitary limit requires the use of advanced methods of many-body theory that can deal with strongly interacting systems. Quantum Monte Carlo methods have proven to be very useful for the calculation of the finite- and zero-temperature equation of state [6, 7, 8, 9] which is found to be in good overall agreement with experimental data [10, 11]. Also, it was possible to predict the effect of the unbalanced population [12] and different masses [13]. More recently, static responses such as the spin susceptibility and spin diffusivity [14, 15] have been measured and also studied theoretically using quantum Monte Carlo (QMC) methods [16] and a diagrammatic approach [17].

Recently, Hoinka *et al.* [18, 19] have measured the dynamic spin and density responses of a Fermi gas at unitarity and in the BEC regime. In order to measure both responses, they used two-photon Bragg scattering, acting on ^{6}Li at very low temperature ($T \sim 0.06\, E_{\rm F}$ at unitarity), and a proper choice of the laser detuning. The density response at unitarity turns out to be significantly different from that of an ideal Fermi gas, showing a clear peak which corresponds to the formation of dimers composed of spin-up and spin-down particles. This signature of dimer formation is not visible in the spin channel, nevertheless the experimental results are quite different from the ideal Fermi gas response. This provides evidence for the importance of correlations in the unitary gas despite its diluteness.

Some of the features shown by the dynamic response function at unitarity were previously determined in theoretical work: at $T = 0$ using a self-consistent mean-field approach based on BCS theory [20], and at $T > 0$ using virial expansions [21]. However, the dynamic properties along the BCS-BEC crossover are not completely understood due to the need of a full many-body theory and the impossibility to use QMC methods for dynamic properties directly. The goal of our study is to utilize successful methods stemming from the many-body theory of strongly interacting systems, combining the virtues of Monte Carlo methods and modern diagrammatic many-body theory, in order to study the dynamic structure function of a low–density gas. For pedagogical material on the techniques to be employed here, see Ref. [22].

2. Dynamic Many-Body Theory

In the present work, we study the density and spin responses of the two-component Fermi gas at unitarity and in characteristic points on both the BEC and BCS sides of the crossover. We use a fully microscopic approach utilizing correlated basis function (CBF) theory [22]. The input to the theory are the ground-state structure functions $S_{\uparrow\uparrow}(k)$ and $S_{\uparrow\downarrow}(k)$ obtained from diffusion Monte Carlo simulations within the fixed-node (FN-DMC) approximation [6]. In these calculations, an attractive square-well potential was used for the interaction. In its most advanced form [23], the dynamic many-body theory (DMBT) used here is the fermion version of the CBF-Brillouin-Wigner perturbation theory previously developed for bosons [24, 25, 26]. The power of DMBT for fermions has been demonstrated by the prediction of a stable roton excitation in two-dimensional ^{3}He, which has independently been confirmed by inelastic neutron scattering experiments [27].

The only further inputs for the calculation of the dynamic response is the fraction of dimers along the BCS-BEC crossover. With that, we obtain a complete description of the density and spin dynamic responses in the momentum-energy plane. In the unitary limit, both theoretical responses are in satisfactory agreement with the recent experimental Bragg scattering measurements [18].

In weakly interacting systems, time-dependent Hartree-Fock (TDHF) theory [28] is a well-established method for capturing the dynamics. The system is subjected to a perturbing Hamiltonian

$$\delta\hat{H}_{\rm ext}(t) = \int d^3r \hat{\rho}^{(\rho/\sigma)}(\mathbf{r}) h_{\rm ext}(\mathbf{r},t)\,; \tag{1}$$

the superscripts ρ and σ stand for density and spin excitations, respectively. $\hat{\rho}^{(\rho/\sigma)}(\mathbf{r})$ is the (spin-)density operator, and $h_{\rm ext}(\mathbf{r},t)$ is a weak, local external field. The wave function resulting from such a perturbation is assumed to be of the form

$$|\psi(t)\rangle = e^{1/2\sum_{ph} c_{ph}(t) a_p^\dagger a_h} |\phi_0\rangle\ , \tag{2}$$

where $|\phi_0\rangle$ is the ground state of a non-interacting system with the same density. The particle ("p") and hole ("h") labels run over spatial quantum numbers and spin degrees of freedom.

The amplitudes $c_{ph}(t)$ are Fourier decomposed

$$c_{ph}(t) = c_{ph}^{(+)}(\omega) e^{-\imath(\omega+\imath\eta/\hbar)t} + c_{ph}^{(-)*}(\omega) e^{\imath(\omega+\imath\eta/\hbar)t}\,. \tag{3}$$

Equations of motion are then derived from a least action principle [29, 30]. They are given by

$$\big(\hbar\omega + \imath\eta - \epsilon_{ph}\big) c_{ph}^{(+)}(\omega) - \sum_{p'h'} V_{ph;p'h'} c_{p'h'}^{(+)}(\omega) - \sum_{p'h'} V_{pp'hh';0} c_{p'h'}^{(-)}(\omega) = 2\int d^3r \rho_{ph;0}^{(\rho/\sigma)}(\mathbf{r}) h_{\rm ext}(\mathbf{r},\omega) \tag{4}$$

$$\big(-\hbar\omega - \imath\eta - \epsilon_{ph}\big) c_{ph}^{(-)}(\omega) - \sum_{p'h'} V_{p'h';ph} c_{p'h'}^{(-)}(\omega) - \sum_{p'h'} V_{0;pp'hh'} c_{p'h'}^{(+)}(\omega) = 2\int d^3r \rho_{0;ph}^{(\rho/\sigma)}(\mathbf{r}) h_{\rm ext}(\mathbf{r},\omega), \tag{5}$$

where $h_{\rm ext}(\mathbf{r},\omega)$ is the Fourier component of the external field. To maintain causality, the real frequency ω is supplemented with a small imaginary contribution corresponding to the adiabatic swichting-on of the perturbation. While usually the limit $\eta \to 0^+$ is performed, we use for η a finite, monotonically increasing function of momentum transfer to phenomenologically incorporate the possibility of excitations to decay. Outside the regime of Landau-damping, this effect is due to multi-pair excitations [23].

From the solutions $c_{ph}^{(\pm)}(\omega)$ we can calculate the (spin-) density response function

$$\chi^{(\rho/\sigma)}(\mathbf{r},\mathbf{r}',\omega) \equiv \frac{1}{\rho(\mathbf{r})\rho(\mathbf{r}')} \frac{\delta \langle\psi|\, \hat{\rho}^{(\rho/\sigma)}\, |\psi\rangle\,(\mathbf{r},\omega)}{\delta h_{\rm ext}(\mathbf{r}',\omega)}\ , \tag{6}$$

and the (spin-)density dynamic structure function

$$S^{(\rho/\sigma)}(\mathbf{r},\mathbf{r}',\omega) \equiv -\frac{1}{\pi}\Im m\chi^{(\rho/\sigma)}(\mathbf{r},\mathbf{r}',\omega) \tag{7}$$

in coordinate space. In a translationally invariant geometry, their momentum space representations, $\chi^{(\rho/\sigma)}(k,\omega)$ and $S^{(\rho/\sigma)}(k,\omega)$, are functions of the momentum transfer k.

The key ingredients of the equations of motion are the matrix elements of the interparticle interaction

$$V_{ph;p'h'} = \left\langle ph'\right| V_{\rm d} \left|hp'\right\rangle - \left\langle ph'\right| V_{\rm ex} \left|p'h\right\rangle \tag{8}$$

$$V_{pp'hh';0} = \left\langle pp'\right| V_{\rm d} \left|hh'\right\rangle - \left\langle pp'\right| V_{\rm ex} \left|h'h\right\rangle \tag{9}$$

and the single-particle spectrum $\epsilon_{ph} = \epsilon_p - \epsilon_h$. In TDHF theory, the potentials $V_{\rm d}$ and $V_{\rm ex}$ are the same and just the bare interaction between the particles, and the ϵ_p, ϵ_h are the Hartree-Fock single-particle energies. However, close to unitarity, our system is strongly interacting and the TDHF approximation is, as we shall see, vastly inappropriate. For such strongly interacting systems like the helium liquids or strongly correlated electrons, CBF theory has proven to be a suitable tool for making quantitative predictions of the dynamic structure function [23], and there is no reason that the method should not be applicable to cold gases.

3. Calculation of the effective interactions

The effective interactions $V_{\rm d}$ and $V_{\rm ex}$ can be derived in basically two different ways: The first, and original derivation [31] was within correlated basis functions theory: CBF theory starts with a correlated ground state

$$|\psi_0\rangle = F\,|\phi_0\rangle \tag{10}$$

where F is a local correlation operator, most frequently taken in the Jastrow-Feenberg form including two- and three- body correlations. This is among others realized in the fixed-node Monte Carlo method for the non-dimerized component, which basically determines the best local correlation operator. Excitations in strongly correlated systems are then treated by generalizing the *ansatz* (2) to

$$|\psi(t)\rangle = Fe^{1/2\sum_{ph} c_{ph}(t)a_p^\dagger a_h}\,|\phi_0\rangle\ . \tag{11}$$

Equations of motion are then derived along the same lines as the TDHF equations (4,5). In a rather intricate diagrammatic analysis [22, 32, 33] one arrives at the same equations of motion (4,5) for a strongly interacting system, the basic difference being that the matrix elements of the bare potential are replaced by correlated matrix elements of the form

$$\left\langle \phi_0 a_{h'}^\dagger a_{p'}\right| F^\dagger(H-E_0)F\left|a_{p'}^\dagger a_{h'}\phi_0\right\rangle \quad \text{and} \quad \left\langle \phi_0\right|F^\dagger(H-E_0)F\left|a_p^\dagger a_{p'}^\dagger a_{h'}a_h\phi_0\right\rangle . \tag{12}$$

These matrix elements can obviously be written as matrix-elements of a two-body operator. A diagrammatic analysis of these interactions [31, 33, 34] leads to the working

formulas for their local parts and, thus, to the replacement of the bare interaction by *effective interactions* $V_{\rm d}$ and $V_{\rm ex}$:

$$\tilde{V}_{\rm d}(k) = \frac{t(k)}{2}\Big(\frac{1}{S^{(\rho)}(k)^2} - \frac{1}{S_{\rm F}(k)^2}\Big)\,, \tag{13}$$

and

$$\tilde{V}_{\rm ex}(k) = -t(k)\,\frac{S^{(\rho)}(k) - S_{\rm F}(k)}{S_{\rm F}(k)^3}\,. \tag{14}$$

where $S_{\rm F}(k)$ is the static structure factor of the free Fermi gas, and $t(k) = \frac{\hbar^2 k^2}{2m}$.

The procedure has been described in pedagogical literature [22] and review papers [34] and does not need to be repeated here. The fixed-node approximation is, for the non-dimerized component, equivalent to the optimized Jastrow-Feenberg method, these are the correct expressions to use.

One can obtain the same quantities from the diagrammatic methods of Feynman-diagram based perturbation theory and the connections between that method and CBF theory unveiled by the parquet-diagram analysis [35, 36, 37]. From that analysis, and by comparing the structure of ring-diagrams in perturbation theory and CBF theory [33], it is known that the Jastrow-Feenberg wave function and, equivalently, the fixed-node approximation, amounts to approximating the Lindhard Function $\chi_0(q,\omega)$ by a "collective" or "mean spherical" approximation (MSA):

$$\chi_0^{\rm MSA}(k,\omega) \equiv \frac{2t(k)}{(\omega+i\eta)^2 - \left(\frac{t(k)}{S_{\rm F}(k)}\right)^2}\,. \tag{15}$$

This approximation for $\chi_0(k,\omega)$ replaces the particle–hole band by an effective collective mode whose energy is chosen such that the first two energy weighted sumrules are fulfilled:

$$\begin{aligned} \Im m \int_0^\infty d\omega\, \chi_0^{\rm MSA}(k,\omega) &= \Im m \int_0^\infty d\omega\, \chi_0(k,\omega)\,, \\ \Im m \int_0^\infty d\omega\, \omega\chi_0^{\rm MSA}(k,\omega) &= \Im m \int_0^\infty d\omega\, \omega\chi_0(k,\omega)\,. \end{aligned} \tag{16}$$

Given a local, effective interaction $\tilde{V}_{\rm d}(q)$, one can construct the static structure function by

$$\begin{aligned} S^{\rm RPA}(k) &= -\int_0^\infty \frac{d(\hbar\omega)}{\pi} \Im m\, \chi^{\rm RPA}(k,\omega)\,, \\ \chi^{\rm RPA}(k,\omega) &= \frac{\chi_0(k,\omega)}{1 - \tilde{V}_{\rm d}(k)\chi_0(k,\omega)}\,. \end{aligned} \tag{17}$$

When the MSA (15) is used, the frequency integration can be carried out exactly and leads to

$$S^{\rm MSA}(k) = \frac{S_{\rm F}(k)}{\sqrt{1 + \frac{2S_{\rm F}^2(k)}{t(k)}\tilde{V}_{\rm d}(k)}} \tag{18}$$

which is seen to be exactly the relationship (13).

The effective interaction in the "direct" channel is particle-hole irreducible, in the exchange channel we must include all particle-hole reducible diagrams. This leads *a priori* to an energy dependent exchange interaction,

$$\tilde{V}_{\rm ex}^{\rm RPA}(k,\omega) = \frac{\tilde{V}_{\rm d}(k)}{1-\tilde{V}_{\rm d}(k)\chi_0(k,\omega)} \tag{19}$$

where in the Jastrow-Feenberg or fixed-node approximation, the Lindhard function $\chi_0(k,\omega)$ is replaced by $\chi_0^{\rm MSA}(k,\omega)$.

The prescription from parquet-theory to make this energy dependent interaction local is as follows: Construct the RPA static structure function by summing the ring diagrams

$$S^{\rm RPA}(k) = -\Im m \int \frac{d(\hbar\omega)}{2\pi} \left[\chi_0(k,\omega) + \chi_0^2(k,\omega)\tilde{V}_{\rm ex}^{\rm RPA}(k,\omega)\right] \tag{20}$$

which leads, when the MSA is used, to Eq. (18). Also, construct the *ladder approximation* for the same quantity in terms of a different and yet unspecified local and energy independent effective interaction, say $\tilde{V}_{\rm L}(q)$

$$\begin{aligned} S^{\rm ladder}(k) &= -\Im m \int \frac{d(\hbar\omega)}{2\pi} \left[\chi_0(k,\omega) + \chi_0^2(k,\omega)\ \tilde{V}_{\rm L}(k)\right] \\ &= 1 - \frac{S_F^3(k)}{t(k)}\ \tilde{V}_{\rm L}(k)\ . \end{aligned} \tag{21}$$

Now choose $\tilde{V}_{\rm L}(k)$ such that $S^{\rm ladder}(k) = S^{\rm RPA}(k)$. This *defines* $\tilde{V}_{\rm L}(k)$. Through the same relationship, we can identify $\tilde{V}_{\rm L}(k)$ with a local, energy independent approximation to $\tilde{V}_{\rm ex}(k,\omega)$. This leads immediately to Eq. (14).

The effective exchange interaction defines the single-particle spectrum

$$\epsilon_k = t(k) - \frac{1}{\nu N}\sum_h V_{\rm ex}(|\mathbf{k}-\mathbf{h}|)\,, \tag{22}$$

where ν is the spin degeneracy. A consistent treatment of both the exchange potential and the single particle spectrum is needed to satisfy the ω^1 sum rule.

We see again, that the analysis of parquet-diagram theory [35, 36] for how to construct the energy independent interactions of CBF theory from the energy dependent vertices of Feynman-diagram based perturbation theory lead to the same results, provided the Lindhard function is replaced by its collective approximation. The above analysis has been carried out only for a very specific class of diagrams, but, since the result is as expected, there is no reason that the analysis should not carry over to other, more complicated structures. Such an analysis is, however, subject to a study in formal many-body theory and beyond the scope of this work.

Our analysis also provides a method to relate methods of diagrammatic many–body theory to Monte Carlo simulation methods: If one neglects, for example, exchange effects,

one can construct $\tilde{V}_{\rm d}(k)$ from the static structure function by demanding that $\tilde{V}_{\rm d}(k)$ reproduces $S^{(\rho)}(k)$ through the ω^0 sum rule

$$S^{(\rho)}(k) = \int_0^\infty d(\hbar\omega) S^{(\rho)}(k,\omega) \ . \tag{23}$$

The prescription provides the *best local* potential that reproduces the known $S^{(\rho)}(k)$. If the fixed-node approximation is used, the relationship (13) is the correct one to use; if the $S^{(\rho)}(k)$ is taken from an improved calculation or from experiment, the full Lindhard function should be used to determine $\tilde{V}_{\rm d}(k)$. We note, however, that the resultant interactions differ only by a few percent.

4. Results

For spin-independent interactions, the spin-density fluctuations depend on $V_{\rm ex}(k)$ but not on $V_{\rm d}(k)$. Thus one might be tempted, as an alternative to using Eq. (14), to construct $V_{\rm ex}(k)$ from $S^{(\sigma)}(k)$ in a similar fashion as $V_{\rm d}(k)$ is derived from $S^{(\rho)}(k)$. Unfortunately, this procedure has numerical difficulties because the resulting problem is very poorly conditioned. We have therefore utilized the local exchange interaction (14). The calculation of the potentials $V_{\rm d}(k)$ (13) and $V_{\rm ex}(k)$ (14) then requires knowledge of no more than the density structure function of the interacting system, $S^{(\rho)}(k)$. For that, we use ground-state results obtained using the FN-DMC method [6], which has proven its accuracy in the description of the BCS-BEC crossover.

The resulting $V_{\rm d}(k)$ and $V_{\rm ex}(k)$ are shown in Fig. 1. The linear behavior at large momenta is related to Tan's relations [38], specifically

$$S^{(\rho)}(k \to \infty) = 1 + \frac{\mathcal{I}}{N}\frac{1}{4k}, \tag{24}$$

where $\mathcal{I}$ is Tan's universal contact parameter and N the number of particles. These lead to the properties

$$\tilde{V}_{\rm d}(k) \sim \frac{\mathcal{I}}{N}\frac{\hbar^2 k}{8m} \qquad \text{and} \qquad \tilde{V}_{\rm ex}(k) \sim \frac{\mathcal{I}}{N}\frac{\hbar^2 k}{8m} \tag{25}$$

which are the cause for the linar increase of the interactions as a function of momentum transfer seen in Fig. 1

For comparison we also display the bare interaction, which corresponds to an attractive square-well potential: $V(r) = -V_0$ for $r < R_0$, and $V(r) = 0$ otherwise. This potential acts only between particles of different spin since s-wave collisions between equal-spin particles are forbidden by the Pauli principle. We use $nR_0^3 = 10^{-6}$ to ensure that the mean interparticle distance is much larger than the range of the potential. The value of the s-wave scattering length is easily changed by modifying the depth V_0 of the potential. Evidently, the bare interaction is much weaker than the effective interaction that is needed to explain the static structure function. This is the compelling evidence alluded to above that the system is in fact very strongly interacting. Note that this is rather different from what one finds in the helium liquids: There, the effective interactions are, in coordinate space, rather similar to the bare interaction except that

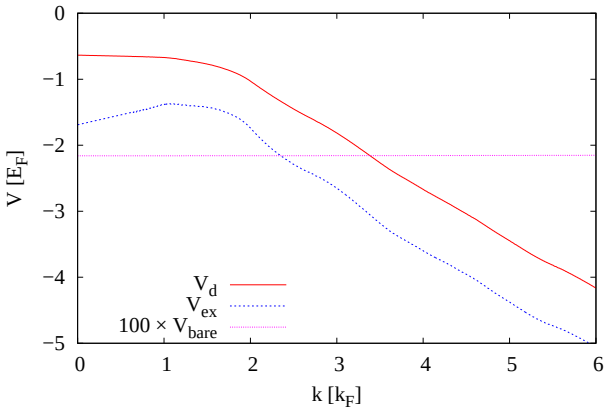

Figure 1. (Color online) Direct and exchange interaction at unitarity ($1/(k_F a) = 0$). The linear behavior at large momenta is a consequence of Tan's relations (24) [38]. The bare potential is much weaker than the effective ones, underlining the strong correlations within the system.

the repulsive hard core is screened off. For a description of the physical effects that determine the properties of these interactions, see Ref. [39].

We have calculated the dynamic structure function in the density and spin channels for $1/(k_{\rm F}a) = -1$ (BCS like), $1/(k_{\rm F}a) = 0$ (unitarity) and $1/(k_{\rm F}a) = 1$ (BEC like) including exchange terms and non-local, energy dependent CBF corrections that have not spelled out explicitly here, see Ref. [33]. Since the system favors, with decreasing $1/(k_{\rm F}a)$, the formation of bound dimers, we consider here a mixture of interacting fermions and non-interacting dimers ("bosons" with $2m$). The relative concentrations by which we weight the two contributions to the dynamic structure function in the density channel are obtained from our FN-DMC ground-state calculations. In particular, the concentration of dimers as a function of the scattering length is estimated assuming that all pairs are in the zero-momentum state. According to this criterion, the concentration of dimers is 100% deep inside the BEC regime and decreases to zero quickly after crossing the unitary limit where it amounts $\sim 50\%$ [40]. Our model cannot predict the width of the "Bose" peak, hence it has been fitted to reproduce the width of the experimental data subject to the constraint that its contribution to the ω^0 sum rule is constant. The spin channel dynamics on the other hand is not affected by the presence of dimers because they do not contribute to spin-density fluctuations.

In Fig. 2, we show results of $S^{(\rho)}(k,\omega)$ and $S^{(\sigma)}(k,\omega)$ for the wave vector $k = 4.2\,k_{\rm F}$. We have selected this particular k value because it is the only momentum measured by Bragg scattering [18]. (This wave vector deviates, due to recalibration of the experimental values [41], slightly from the wave number $k = 4.5\,k_{\rm F}$ reported in Ref. [18].) In agreement with the experimental data, the density channel of the dynamic structure function shows a clear "Bose" peak centered at energy $\hbar^2 k^2/4m$ coming from the scattering off the ↑-↓ pairs. At higher energies, contributions from single Fermi

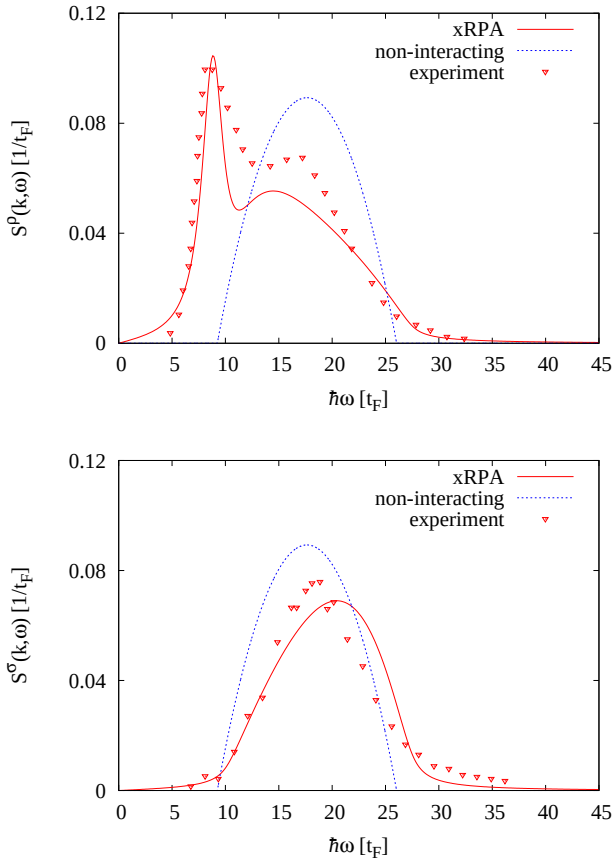

Figure 2. (Color online) The dynamic structure function in the density (*top*) and spin (*bottom*) channels at unitarity ($1/(k_F a) = 0$) and at a momentum $k = 4.2k_F$ (solid line). The damping constant for this momentum transfer was chosen $\eta \approx t_F$. The points are the experimental data of Ref. [18]. Dashed line stands for the non-interacting response.

atoms appear as a broader response. The importance of correlations at unitarity is best demonstrated by comparing the response coming from the full theory with the non-interacting Lindhard function, also shown in Fig. 2. Our result for the spin channel at unitarity and the same k value as in the experiment is also shown in Fig. 1 (bottom panel). As mentioned above, dimers do not contribute to the spin channel and only atomic contributions appear. As in the density channel, the use of many-body theory is crucial to describe the experimental data, note that the response of a non-interacting system has a completely different structure and differs substantially from what was observed in the experiment.

The full energy-momentum dependence of the density and spin response functions is shown in the form of stacked line plots in Fig. 3. At low momenta, $k \lesssim 4k_F$, the dimer peak lies inside the particle-hole ($p-h$) band and has a large overlap with the single-atom

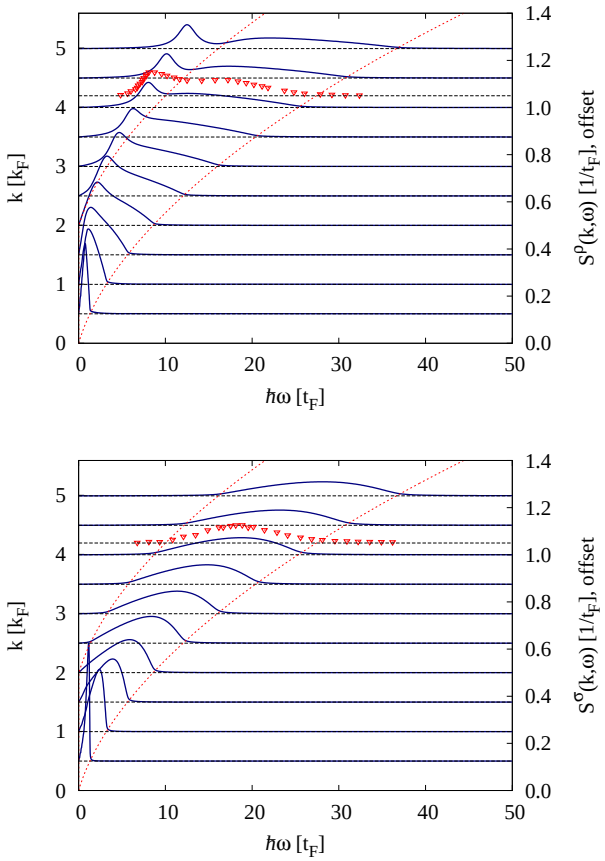

Figure 3. (Color online) The figure shows line plots of the dynamic structure function in the density (*top*) and spin (*bottom*) channels at unitarity ($1/(k_F a) = 0$) as a function of the momentum transfer k and energy transfer $\hbar\omega$ in units of the Fermi energy $E_{\rm F}$. The left vertical scale shows the momentum offset, the right scale the value of $S^{\rho,\sigma}(k,\omega)$. The dashed lines show the limits of the particle-hole band. The triangles correspond to the momentum transfer at which the experiment of Ref. [18, 41] was performed.

scattering contribution. At higher momenta, the "Bose" peak is progressively decoupled of Fermi excitations with a position given by half the recoil energy. The strength of the spin response is localized inside the $p-h$ band but interactions make the peak slightly asymmetric and shifted to higher energy compared with the non-interacting response; this effect is washed out at momenta $k \gtrsim 4k_F$.

Bragg scattering [18, 19] was also applied to a point in the phase diagram located inside the BEC side, in particular at $1/(k_F a) = 1$, whereas no experimental data exists on the BCS side. We have applied dynamic many-body theory to the experimental BEC point and to the symmetric one in the BCS side, with $1/(k_F a) = -1$, and at a momentum transfer $k = 4.2k_F$. The response in the BCS regime is rather close to that of

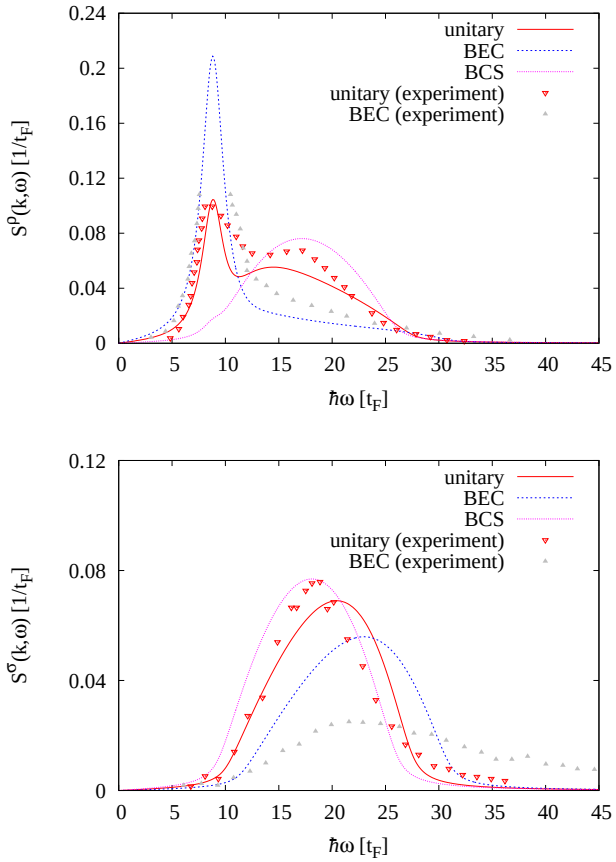

Figure 4. (Color online) The dynamic structure function in the density (*top*) and spin (*bottom*) channels at unitarity ($1/(k_F a) = 0$), BEC ($1/(k_F a) = 1$), and BCS ($1/(k_F a) = -1$). The lines are results from dynamic many-body theory and points are experimental data of Ref. [18]. All data corresponds to $k = 4.2 k_F$.

the free Fermi gas, with only an incipient Bose peak from the dimer contribution due to its very low concentration (< 10 %). On the contrary, the dimer contribution dominates the density channel in the BEC side since the concentration of dimers is ~ 90 %. Our theory, which produces results in good agreement with experiment in the unitary limit, seems to worsen in the BEC regime. This is seen most clearly in the spin response at $1/(k_F a) = 1$ where our result does not show the broad response obtained from Bragg scattering.

5. Conclusion

To conclude, motivated by the first measurements of the dynamic structure function of a two-component resonantly interacting Fermi mixture, we have employed a well-tested theory able to predict its dynamic response. Dynamic many-body theory has been used

together with a FN-DMC input for the static structure factor. From a direct comparison with experimental data [18], we show that the ideal Fermi gas model is not sufficient to reproduce correctly the dynamic response functions. We have formulated a description in terms of a mixture of dimers (bosons) and atoms (fermions). This simple model permits to capture correctly the complicated structure of the density response at the unitary limit. Our theory departs from the experimental data, mainly in the spin channel, when the fraction of dimers is large. Finally, we provide information on the dynamic response for different (previously not measured) values of the momentum in the unitary limit and on the BCS (not measured) side.

We acknowledge partial financial support from the DGI (Spain) Grant No. FIS2011-25275 and Generalitat de Catalunya Grant No. 2009SGR-1003 as well as from the Austrian Science Fund FWF under project I-602. G. E. A. acknowledges support from the Spanish MEC through the Ramon y Cajal fellowship program. Additional support was provided by a grant from the Qatar National Research Fund # NPRP NPRP 5 - 674 - 1 - 114.

[1] Giorgini S, Pitaevskii L P and Stringari S 2008 *Rev. Mod. Phys.* **80** 1215
[2] Zwierlein M W, Schirotzek A, Schunck C H and Ketterle W 2006 *Science* **311** 492
[3] Partridge G B, Li W, Kamar R I, Liao Y and Hulet R G 2006 *Science* **311** 503
[4] Shin Y, Schunck C H, Schirotzek A and Ketterle W 2008 *Nature* **451** 689
[5] Navon N, Nascimbene S, Chevy F and Salomon C 2010 *Science* **328** 729–732
[6] Astrakharchik G E, Boronat J, Casulleras J and Giorgini S 2004 *Phys. Rev. Lett.* **93** 200404
[7] Carlson J and Reddy S 2005 *Phys. Rev. Lett.* **95** 060401
[8] McNeil Forbes M, Gandolfi S and Gezerlis A 2011 *Phys. Rev. Lett.* **106** 235303
[9] Drut J E, Lähde T A, Wlazłowski G and Magierski P 2012 *Phys. Rev. A* **85** 051601
[10] Nascimbène S, Navon N, Jiang K J, Chevy F and Salomon C 2010 *Nature* **463** 1057
[11] Ku M J H, Sommer A T, Cheuk L W and Zwierlein M W 2012 *Science* **335** 563
[12] Pilati S and Giorgini S 2008 *Phys. Rev. Lett.* **100** 030401
[13] Astrakharchik G E, Giorgini S and Boronat J 2012 *Phys. Rev. B* **86** 174518
[14] Sanner C, Su E J, Keshet A, Huang W, Gillen J, Gommers R and Ketterle W 2011 *Phys. Rev. Lett.* **106** 010402
[15] Sommer A, Ku M, Roati G and Zwierlein M W 2011 *Nature* **472** 201
[16] Wlazłowski G, Magierski P, Drut J E, Bulgac A and Roche K J 2013 *Phys. Rev. Lett.* **110** 090401
[17] Palestini F, Pieri P and Strinati G C 2012 *Phys. Rev. Lett.* **108** 080401
[18] Hoinka S, Lingham M, Delehaye M and Vale C J 2012 *Phys. Rev. Lett.* **109**(5) 050403
[19] Hoinka S, Lingham M, Fenech K, Hu H, Vale C J, Drut J E and Gandolfi S 2013 *Phys. Rev. Lett.* **110** 055305
[20] Combescot R, Giorgini S and Stringari S 2006 *Europhys. Lett.* **75** 695
[21] Hu H and Liu X J 2012 *Phys. Rev. A* **85** 023612
[22] Fabrocini A, Fantoni S and Krotscheck E 2002 *Introduction to Modern Methods of Quantum Many–Body Theory and their Applications* (*Advances in Quantum Many–Body Theory* vol 7) (Singapore: World Scientific)
[23] Böhm H M, Holler R, Krotscheck E and Panholzer M 2010 *Phys. Rev. B* **82** 224505/1–28
[24] Jackson H W and Feenberg E 1961 *Ann. Phys. (NY)* **15** 266–295
[25] Jackson H W and Feenberg E 1962 *Rev. Mod. Phys.* **34** 686–693
[26] Chang C C and Campbell C E 1976 *Phys. Rev. B* **13** 3779–3782
[27] Godfrin H, Meschke M, Lauter H J, Sultan A, Böhm H M, Krotscheck E and Panholzer M 2012 *Nature* **483** 576579
[28] Thouless D J 1972 *The quantum mechanics of many-body systems* 2nd ed (New York: Academic Press)
[29] Kerman A K and Koonin S E 1976 *Ann. Phys. (NY)* **100** 332–358
[30] Kramer P and Saraceno M 1981 *Geometry of the time-dependent variational principle in quantum*

mechanics (*Lecture Notes in Physics* vol 140) (Berlin, Heidelberg, and New York: Springer)
[31] Krotscheck E and Clark J W 1979 *Nucl. Phys. A* **328** 73–103
[32] Chen J M C, Clark J W and Sandler D G 1982 *Z. Physik A* **305** 223–229
[33] Krotscheck E 1982 *Phys. Rev. A* **26** 3536–3556
[34] Krotscheck E 2000 *J. Low Temp. Phys.* **119** 103–145
[35] Jackson A D, Lande A and Smith R A 1982 *Physics Reports* **86** 55–111
[36] Jackson A D, Lande A and Smith R A 1985 *Phys. Rev. Lett.* **54** 1469–1471
[37] Krotscheck E, Smith R A and Jackson A D 1986 *Phys. Rev. A* **33** 3535–3536
[38] Tan W C and Inkson J C 1999 *Phys. Rev. B* **60** 5626
[39] Aldrich C H and Pines D 1976 *J. Low Temp. Phys.* **25** 677–690
[40] Astrakharchik G E, Boronat J, Casulleras J and Giorgini S 2005 *Phys. Rev. Lett.* **95** 230405
[41] Hoinka S 2013 (private communication)